Long-period oscillation in the magnetic coupling through chromium in a magnetic multilayer: Bulk issues

Dale D. Koelling
Materials Science Division, Argonne National Laboratory, 9700 South Cass Avenue, Argonne, Illinois 60439-4845
(Received 10 September 1998; revised manuscript received 4 November 1998)

The long period oscillation of magnetic coupling through Cr as the spacer layer of especially Fe/Cr magnetic multilayers is examined. It is shown that a reasonable empirical adjustment of the *d*-band position does bring calipers on the *N*-centered ellipses into agreement with experiment. The lens surface becomes too small and more anisotropic providing further evidence that it is not involved. However, the neck of the jack surface does reach the proper size and so accounts for the photoemission observations. A mechanism of mode coupling to enhance the strength of the long period oscillation is examined and rejected. A thorough examination of the Cr/(V,Mn) alloy spacer data strongly suggests instead a predilection for mode exclusion. [S0163-1829(99)00309-4]

I. INTRODUCTION

Among the artificial magnetic multilayer systems that exhibit giant magnetoresistance, the Fe/Cr system is very special. One of the earliest discovered[1] and most thoroughly examined,[2–5] this system comes closest to perfect matching of atomic spacing between the individual layers ($a_{Cr}=5.44$ au$=2.88$ Å vs $a_{Fe}=5.41$ au$=2.86$ Å). Deleterious lattice strain effects are thereby minimized. Alas, there is, as usual, a price to pay: interdiffusion easily occurs at the interface — requiring careful management.[6] Fe/Cr is also very special because it exhibits at least two periods (repeat distances): One of the shortest, at two monolayers; and one of the longest, at about 18 Å. The short period arises from Fermi-surface nesting also associated with the spin-density wave in the bulk. The short period quickly disappears if the interface quality is not carefully maintained[7–10] as a result of phase cancellations.[11–13]

For our purposes, this is actually a benefit, as it permits direct examination of the long period—which is the focus here. There are two good reasons to carefully examine that period. First is that it has very significant implications: Nearly all observed periods fall in the range of 9–11 Å,[14] so long periods acquire general interest. The most credible explanation for this narrow range is that it is merely a reflection of a window of opportunity. The cutoff at short range is quite easily understood. Periods smaller than the observed range correspond to only a repeat distance of only 2 or 3 monolayers. Coupling is strongly suppressed by surface roughness or interdiffusion which generally occurs over such distances. (Note that this is another way in which Fe/Cr is special: it does exhibit such a short repeat distance.) A window-of-opportunity type explanation also requires that the range be cut off at the larger distances. The natural assertion is that long periods are difficult to observe because the coupling effect decays with distance. Assuming a point Fermi-surface caliper or Kohn anomaly, the coupling should decay as the inverse square of the spacer thickness d.[15,16] The coupling will decay more slowly (as d^{-1}) if there is actual Fermi-surface nesting—which is the case for the Cr short period, being related to the same Fermi-surface nesting as the bulk spin wave—but such is not the case for the long-period. Hence, the desire to understand the cutoff of longer-ranged periods gives added significance to the question why the Cr long period is so robust. One would like to use the exception to prove the rule, so the long-period oscillation of Fe/Cr becomes quite interesting on this basis alone. It is not completely unique: Co/Ag exhibits a 16 Å repeat distance,[17] for example. But it is a member of a very restricted class.

And second, the origins of this long period are only beginning to become clear. There have been multiple hypotheses offered for its occurrence.[18–23] However, it is apparent that the Cr long period can indeed be associated with a macroscopic Kohn anomaly from Cr bulk metal. Because of our interest in the bulk issues, this effect is viewed as providing the coherent coupling through the Cr spacer layer which must then amplified by the reflection properties at the Fe interfaces[16,24,20–22] (quantum-well considerations).

There are several very important experimental observations to consider: (1) the Cr long period's existence in multiple directions;[25] and (2) the observation of (possibly) related quantum well states in the (100) direction by photoemission;[26] and (3) persistent existence of the period with vanadium and manganese alloying;[27] and (4) its robust character.

The Cr long period exists at the same repeat distance of 18 Å for both the (100) and the (211) directions.[25,28] Although experimental problems exist for the (110) direction,[29,30] a significantly long, albeit somewhat shorter, period occurs in that direction as well.[14,27] The long period also persists in polycrystalline Fe/Cr samples with an 18 Å repeat distance which, if the polycrystals do not exhibit a few favored orientations, would imply a very isotropic origin. The existence of this long period in multiple directions rules out numerous hypotheses concerning its origin. The very near constancy between (100) and (211) puts some pretty severe restrictions on a Kohn-anomaly interpretation. Given standard band-structure results, this similar occurrence in all three directions suggested the possibility that the spanning vectors occur on a small surface occurring along the (100)

directions known as the lens.[19] This lens is a small Fermi-surface piece arising from the interaction of a large Γ-centered piece (jack body) with a modest sized ellipse occurring along the (100) directions (jack knob). These two surfaces interact to form the famous Fermi-surface jack together with the small lens occurring within the juncture of the jack body and its knob. In standard local-density-approximation (LDA) calculations, the lens has nearly the correct size and shape to account for the observed behavior. However, it has a very low local joint density of states (mass factor) suggesting very weak intensity. States on this surface are of almost pure *d*-wave function character; a concern because *s*-*p* character (only *p* character is available at the Cr Fermi surface) is favored for observable coupling both because these states are more robust against scattering losses[19] in the bulk and because they exhibit the best surface reflection with the iron.[20–22] Nonetheless, photoemission does observe quantum-well states in the vicinity of the lens.[26] And, obviously, *d*-state based coupling cannot be casually ruled out in Cr since it occurs in the short period oscillation. The long period is unlikely to have the short period's benefit of full surface nesting, certainly not for the lens as an origin, so this cannot be a serious proposal for an alternative. It will be seen shortly that the lens is also just too small, although other nearby possibilities exist. Still, one must proceed with caution: one cannot ''cavalierly'' discard the lens in spite of all its deficiencies. In Co/Cr multilayers,[5] the repeat distance is increased to 21 Å more nearly what is found for the lens in the adjusted calculations of Sec. II.

A more consistent picture assumes that spanning vectors on the *N*-centered ellipses are the origins of the long period.[20–22] The *N* ellipse Fermi-surface pieces arise from hybridized *p*-*d* wave function character and so satisfies criteria for robustness and good reflection properties. In a straightforward local-density approximation (LDA) calculation, the *N*-centered ellipses are unfortunately too large. However, it is known that the relative positioning of the *s*-*p* and *d* states is slightly in error when applying the LDA for elements occurring in the center of the transition series, and especially the 3*d* series. By examining the experimental data[31] for the size of these surfaces, it is found[20] that the *N* ellipses are somewhat smaller than calculated and can indeed yield calipers of the correct size in all three directions. This is consistent with improvements found for Nb (Ref. 19) using an empirical adjustment for relative positions of the *p* and *d* orbitals. The adjustment employed was developed explicitly for Fermi-surface studies[32,33] but then found to improve other properties as well.[34] One might well ask whether the same procedure will improve the results for Cr. So, an empirically adjusted calculation similar, but not identical, to that employed for Nb is presented in Sec. II. Calculations of this type are known in other contexts since (1) such adjusted calculations are closely related to the constrained variational calculations that are performed as part of ''LDA+U'' analyses,[35] and (2) in the form used here, it becomes a simplified form of the state-dependent-potential model.[36] Section II first examines how well the ellipses serve as possible origins of the observed repeat distances (spanning vectors) and then looks to see what occurs in the lens/jack-neck region. The ellipses prove out reasonably well, although some improvement could be desired (as always). But this does not eliminate interest in the lens regime since similar spanning vectors occur in that region.

Just what should be made of the quantum-well states observed in that region by the photoemission experiments?[26] Are they to be abandoned as superfluous artifacts?[20,21] Perhaps that would be a bit too hasty. Since they have been seen to exist, is it possible they could act in concert to enhance the strength of the coupling? Normally, the oscillating behavior, in the asymptotic regime, is a sum of terms:

$$I = I_o(d) + \sum_\alpha I_{\mathbf{q}_\alpha}{}^\alpha(d), \tag{1a}$$

$$I_{\mathbf{q}_\alpha}{}^\alpha(d) = \frac{-Zm_\alpha{}^*}{d^2} F_\alpha(d,T)\sin(q_\alpha d + \psi_\alpha), \tag{1b}$$

$$m_\alpha{}^* = \frac{|\kappa_x{}^\alpha \kappa_y{}^\alpha|^{1/2} v_z{}^\alpha}{|v_z v_z'|}, \tag{1c}$$

$$F_\alpha = \frac{(d/L_\alpha)}{\sinh(d/L_\alpha)}, \tag{1d}$$

$$L_\alpha(T) = \frac{v_z^\alpha}{2\pi(T+T^*)}. \tag{1e}$$

q_α is the extremal caliper connecting two points on the Fermi surface: i.e., $dq_\alpha/dk_\parallel = 0$ for $k_\parallel$ along the layers. Note that any quantity labeled with an α involves both Fermi-surface points. v's are velocities with

$$(v_z{}^\alpha)^{-1} = [v_z{}^{-1} + v_z'^{-1}]/2, \tag{2}$$

and $\kappa_{x/y}$ are the eigenvalues of the curvature matrix perpendicular to q_α. The effective mass m_α^* is a local joint density of states about the caliper that is often referred to as the geometrical factor. A slight improvement in its determination is outlined in the Appendix. A Dingle-Robinson temperature has been incorporated into the coherence length L_α to account for scattering in the bulk of the spacer. The same scheme cannot incorporate the interface effects. Both a Ruderman-Kittel-Kasuya-Yosida (RKKY)-type treatment[15] and a quantum-well-type treatment[37–39] arrive at this form in the asymptotic regime although the quantum-well formulation will exhibit a more complex form for the decay than d^{-2}. In the RKKY formulation, a $1/d$ arises from the integration along q_α and this is the factor that differs. Two factors of $d^{-1/2}$ arise from each of the perpendicular integrals as a component of how rapidly phase coherence is lost in that direction. So it will not appear for each direction in which there is nesting. Hence, $d^{-3/2}$ drop off for line nesting and $1/d$ drop off for full planar nesting. The factor Z involves the interfaces and may be written in terms of reflection coefficients there. Actually, neglecting the content of Z is much like performing a generalized susceptibility calculation which focuses on phase-space effects alone.

When calculating the strength of the interactions, one includes the geometric multiplicity (number of equivalent spanning vectors) in determining the strength of the coupling. That multiplicity factor actually represents the coupling together of degenerent interactions. It is easily accom-

modated since the surface reflection terms, at least for the ideal surfaces, are also identical and this becomes a simple extension of the discussion for the rates of drop off. But what about degenerent modes even when the spin asymmetry of the reflection is not so favorable? Even for the perfect model, they are involved in the relevant component of the susceptibility. And if one adds possible coupling channels due to rough, imperfect surfaces, to mismatch strains and dislocations, and so on, then the possibility to couple in these addition modes is significant. This can be expected to increase the strength of the coupling. The possibility that one could have mode coupling is especially interesting since one issue is the strength of the long period.

V and Mn alloyed spacer systems are examined in Sec. III. Vanadium alloying experiments give the strongest evidence against the lens as the sole origin of the long period: As V is alloyed into Cr, the lens actually vanishes, yet the long period persists at least in the $\langle 110 \rangle$ direction. So although the lens-jack regime can be pretty well ruled out as the sole cause of the long period for Fe/Cr, it is further examined here as a possible enhancing mechanism through mode coupling.

The effect of the interfaces is considered with a somewhat different view in the Sec. IV. Of course, part of the motivation is the strong effect that surface roughness is seen to have on the calculated amplitudes.[27,22] But a more interesting question arises from the observation that a CsCl structure might be significant for analyzing this long period.[23] The original observation pointed to the possible existence of antiferromagnetic couplings. However, for the $\langle 100 \rangle$ direction considered, the boundary surfaces can induce a similar symmetry-breaking coupling. This intriguing possibility generally has not been incorporated in analyses performed and is examined in Sec. IV.

II. ADJUSTED MODEL CALCULATIONS

In this section, multilayer systems involving Cr spacer layers will be analyzed in terms of Kohn anomaly spanning vectors, but incorporating an empirical correction for slight inaccuracies of the LDA. A similar adjustment has already been seen to improve the results for Nb.[19] Because the calculations presented are bulk calculations, effects of the surface properties[20] and the quantum-well states[34] that can result must be considered separately. The focus in this section is the examination of the changes induced on the available Kohn anomalies by the correction being applied.

The empirical adjustment applied is based on the observation that the most sensitive deficiency of the LDA is relative band placement. Bands derived from different atomic angular momentum (l) character are shifted relative to one another due to the (minor) inadequacies of the LDA potential. Because of Fano antiresonance, the only wave function character found at the Cr Fermi surface derives from d orbitals with small, but crucial, p orbital admixture, primarily on the N-centered ellipses (see Fig. 1). Thus we are concerned about the relative placement of the p and d orbitals. Limiting our interest to the Fermi surface, energy shifts of these orbitals are the only two possibilities for a simple adjustment. Either, but not both, can be adjusted to see if we can accomplish our goal.

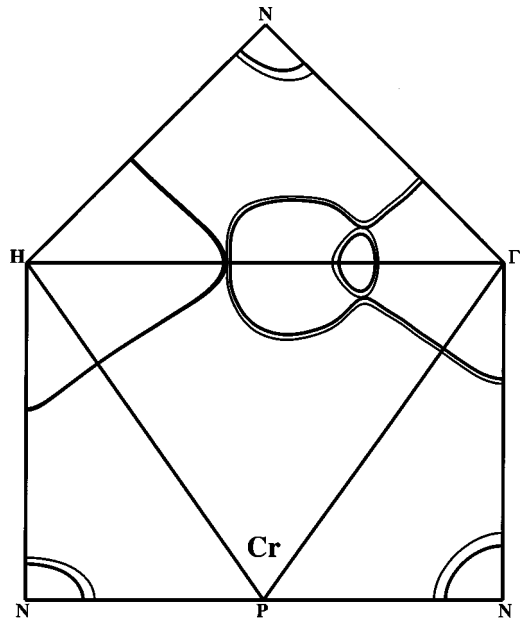

FIG. 1. Intersection of the Fermi surface with the bounding planes of the Brillouin zone. The Fermi surface shown as the heavier line results when the optimal adjustment ($V_\delta = 0.05$ Ry) has been incorporated. See text. The unadjusted surface is shown as the lighter line. All three cross sections of the small (hole) ellipses located at the N points are seen. Note that these ellipses are *not* spherical. The octahedron centered at H reaches out and almost touches the Γ-centered jack along the Γ-H line. The separation is actually a result of the spin-orbit coupling. The lens is clearly seen along that line lying just at the constriction of the jack. This is mandated by the obvious anticrossing separation that converts what would otherwise be an octahedron about Γ and an elliptical surface at ''X,'' half way between Γ and H, into the jack and the lens.

Because the p character arises as an admixture from higher lying bands (remnant of the plane-wave band), it seems most natural to adjust the position of the p orbitals. That is the choice made previously for Nb.[32,33,19] However, because the Cr 3d states are almost completely contained within the nonoverlapping spherical (muffin tin) region that surrounds each atomic site, the adjustment might be easier to understand if it is instead applied to the d orbitals, which is what is done here. Certainly, it is easier to relate it to the constrained variation calculations used for LDA+U. While the comparison to LDA+U has been omitted for brevity, it is interesting to note two results that do appear when such a comparison is made. First, the d-count within muffin-tin spheres that results at the optimally adjusted shift is 3 for V and 4 for Cr. In fact, the adjustment could have been done about as well by just imposing the d-count restriction instead. Interesting as it is, that observation requires serious thought. Second, from the process, it is possible to extract screened U values for the model where only the d orbitals are correlated in the sense of having a nonzero U in a model Hamiltonian. The values resulting are 3.5 eV for V and 5.1 eV for Cr.

Choosing to incorporate the empirical correction by adjusting the placement of the d orbitals, one ends up performing calculations on a simplified form of the state-dependent-potential model specifically introduced for V and Cr,[36] which also focused on the N ellipse size and shape. The state-

dependent-potential model has been extensively explored for the bcc transition metals V,[36,40–42] Cr,[36,41,43] Mo,[43] and Nb.[40,44] Calculations were performed using the X_α model in a muffin-tin shape approximation with the addition of a potential of 0.05 Ry for the t_{2g} (their $d\varepsilon$) orbitals and of 0.09 Ry for the e_g (their $d\gamma$) states. The results were adjusted using the de Haas–van Alphen data for V and applied to both Cr and V. X-ray form factors were examined and found to be dramatically improved although large discrepancies remained for V. Those results definitely harbinger success.

To shift the *d*-derived states relative to the remaining (especially *p*) states, we introduce an extra (empirical) ''semilocal'' potential which, in its simplest form, is

$$V_a(\mathbf{r}) = V_\delta \sum_m |lm\rangle\langle lm|, \tag{3}$$

where $|lm\rangle = \Theta(r-R)\times Y_l^m(\hat{r})$ and the projection is defined using a three-dimensional (3D) integral over a sphere of radius *R*. Clearly, when *R* is set equal to the muffin-tin radius R_{MT} in any band-structure method that uses augmenting orbitals within that sphere, implementation becomes trivial: One merely carries through the calculation in a completely standard fashion *except* that, for the given l, ε_l, the orbital energy to solve for the augmenting function, is replaced by $(\varepsilon_l + V_\delta)$ in the construction of the Hamiltonian matrix. In the calculations reported here, the linear-augmented plane-wave (LAPW) method is used, so this potential is easily accommodated. Implementation only requires a minor exercise in bookkeeping plus having to reconverge the self-consistency process—for each parameter choice. Calculations are performed in the warped muffin-tin (WMT) approximation: the density and potential are spherically averaged within the muffin-tin sphere but fully described outside. One must consider that this has consequences which appear below.

Several other aspects of calculational technique are also worthy of note. All calculations, including the self-consistency iterations, incorporated spin-orbit coupling via a second variational treatment[45] because it results in a separation of the lens and the jack — an important issue in this study. Calculations were performed with tighter tolerances appropriate for examination of the smaller features relevant to the long period. Self-consistency was pushed to the limit that no change occur within the print format normally used: <0.01 for the radial density within the spheres and <0.1 for all Fourier components within the interstitial region (multiplied by the unit-cell volume). The irreducible wedge of the Brillouin zone was sampled at 506 points—a cubic grid with a $\pi/10a$ linear spacing. Thus, since 18 Å represents $3.2\times(\pi/10a)$, all results are thus extremely closely tied to the (almost) *ab initio* calculation. This same grid of points was used as the basis for a Fourier spline[46–48] interpolation. That interpolation utilized a total of 910 star functions (the plane waves corresponding to all lattice vectors interrelated by the symmetry operations of the cubic group are incorporated into a single symmetrized star function). The interpolation scheme is constrained to pass through all data points and the extra freedom arising from surplus of functions is used to smooth the variation between points. The star functions represent all plane waves within a cube with a half-side

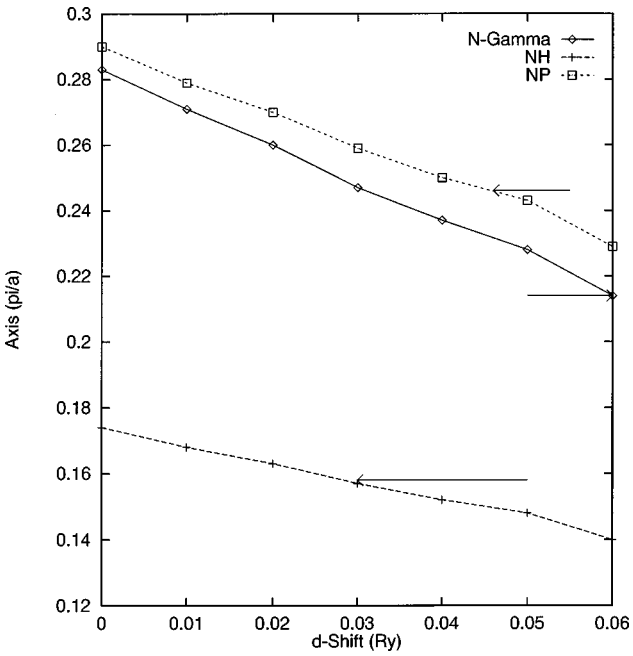

FIG. 2. Variation of the half principle axes of the ellipses due to the empirical adjustment value V_δ. The short principal axis (NH) achieves the experimental value for an adjustment of 0.03 Ry. The longest principal axis (NP) value crosses its experimental value between 0.04 and 0.05 Ry while the ($N\Gamma$) value crosses at 0.06 Ry. The smaller slope of the (NH) curve makes 0.05 Ry a reasonable compromise. [Lengths extracted from experiment are 0.173, 0.234, and 0.268 Å^{-1} or 0.158, 0.214, and 0.246pi/a (Ref. 31)].

dimension of $16a$. This means that the data points *must* be separated by a distance of $\pi/16a$ or the procedure will experience singular matrices resulting from inconsistency with the requirement that it be able to pass the curve through all data points *no matter what the value*. The choice of cubic truncation is motivated by the desire to have all three directions independently resolved to this precision.

While the incorporation of V_δ into the calculation is quite easy, the actual assignment of its value, and the interpretation of that value, are a bit more involved. The approach taken adjusts V_δ so that, as best possible, the resultant band structure produces the same ellipsoidal axes as found for the experimentally-derived[31] *N*-centered ellipses. That band structure is then examined to see whether the observed Kohn anomalies (repeat distances) are indeed found and how they might arise. To determine V_δ, a simple search was performed by trying values that varied by increments of 0.01 Ry in the range between zero and 0.10 Ry. The most appropriate value was found to be 0.05 Ry, as can be seen from Fig. 2. Obviously, the adjustment does not solve all problems and so results in a spread of optimal V_δ values. To put this in context, the experimental semimajor axes were not plotted in Fig. 1 because they could not be clearly distinguished from the adjusted surface: being slightly outside (larger) along N-H and N-P and inside (smaller) along N-Γ.

Adjustment to the vanadium data is a more reliable procedure in that it is *real* data: the Cr calipers are actually extracted data from Cr measurements in the presence of the spin-density wave requiring the use of an ellipsoidal shape approximation (which we will see to be weak). Table I

TABLE I. Adjustment of V_δ for vanadium by comparison of calculated extremal areas for the *N*-centered ellipses with the experimental values of Ref. 49. Orbits are identified by their field direction. The ⟨100⟩ orbits are distinguished by their degeneracies: the twofold degenerate occurs in the basal plane whereas the other occurs perpendicular to that plane in the zone face. The ⟨110⟩ orbits are the fourfold degenerate, or canted, orbit that does not fall in the basal plane, the zone face (ZF) orbit with its field along the *H*-*N* line, and the straight out (SO) field along the Γ-*N* line. Units used are (atomic units)$^{-2}$ for consistency with Ref. 36 and 50.

Orbit	No Adj.	$V_\delta=0.04$	$V_\delta=0.05$	$V_\delta=0.06$	Expt.
⟨100⟩ 2	0.202	0.177	0.168	0.160	0.161
⟨100⟩ 1	0.171	0.149	0.140	0.133	0.141
⟨110⟩ 4	0.172	0.152	0.144	0.137	0.144
⟨110⟩ (ZF)	0.225	0.197	0.187	0.178	0.179
⟨110⟩ (SO)	0.183	0.163	0.155	0.148	0.149

shows the results of current calculations. Clearly the best adjustment is between $V_\delta=0.05$ Ry and $V_\delta=0.06$ Ry. It is on this basis that the value of 0.05 will be used across the the alloy series in the calculations for the next section.

The current results can be seen to be consistent with those of the state-dependent-potential model as follows. A degeneracy weighted average of the two shifts used in the state-dependent-potential is 0.066 Ry. A pretty good guess for the effective α to use in an X_α treatment to match the current exchange-correlation calculation is $\alpha=0.72$. Increasing α will pull the *d* states down relative to the *sp* states. Thus the average upward shift must be larger for the state-dependent-potential calculation than for the current one. The 0.04 Ry splitting found in the state-dependent-potential model is a bit harder to reconcile — the value of zero has been used here, which is clearly too small but consistent with what is being sought. Further, this splitting of the *d*'s should have no reduction from the size of the potential to the eigenvalue effect as in the case of the *d*-*sp* shift. Consequently it is a really large effect. How much of it is due to the shape approximations used and how much due to orbital effects?[51] For the case of the state-dependent-potential calculation using a muffin-tin potential, one expects a very strong component of the effect to be due to the shape approximation. Yet the form-factor calculations[42] would accommodate an even larger splitting. But, examination of Table I would suggest another scenario. Note that the various orbit areas are matched either for $V_\delta=0.05$ or $V_\delta=0.06$ suggesting that, for the current calculations, an applied splitting of 0.01 Ry would be quite adequate. The warped muffin-tin approximation employed here incorporates variations (''asphericity'') in the interstitial region outside the muffin-tin spheres but retains the spherical approximation inside those spheres that enclose the atoms. The interstitial region has been shown to contribute the larger effect and the remaining difference is near what would be expected from the nonspherical terms. It is perhaps a bit large but the question of what level contribution really arises from the orbital effect should not be addressed without switching to full potential calculations.

Table II lists the resulting Kohn-anomaly spanning vectors that could be germane to the long period oscillation. For simplicity, all information about reciprocal space distances will be reported as a wavelength in Ångstroms: Vector lengths are given as $\lambda=2\pi/q$ ($=2a/\tilde{q}$ with q expressed in π/a units). It has the advantage of keeping focus on the target repeat distance but requires care in discussion since the wavelength has a reciprocal relation to the quantities actually calculated. It is necessary to be explicit which is being considered, since different choices invert the meaning of smaller and larger.

First, how well does the adjustment actually work? As noted above, the agreement for the ellipse calipers is good enough to be difficult to exhibit graphically. That agreement can be better probed by comparing the ''dHvA'' column of Table II with the two calculated repeat distances [i.e., $\lambda(0.00)$ and $\lambda(0.05)$]. The adjustment has clearly improved the size of the ellipses, and a finer adjustment of V_δ could do even better. But what about the anisotropy? In the basal plane, the experimental ratio is $\lambda_{NH}/\lambda_{N\Gamma}=1.36$ while the unadjusted ratio is $\lambda_{NH}/\lambda_{N\Gamma}=1.62$ and the adjustment has only brought the ratio down to $\lambda_{NH}/\lambda_{N\Gamma}=1.55$. In reciprocal space, the ellipse is is too large perpendicular to the zone face (*N*-Γ) and too small along the basal plane in that face (*N*-*H*). Also, the interpretation of the de Haas–van Alphen (dffvA) data suggests that the ellipse should be slightly elongated: a slightly longer, by about 25%, semimajor axis along *N*-*P* than perpendicular to the zone face (*N*-Γ). The calculation has these two axes essentially identical in the unadjusted calculation and reaching a ratio increased by only 6% in the adjusted calculation. So, while the adjustment has improved the size, it has done but little for the anisotropy. To improve the anisotropy, one would either have to incorporate the relative t_{2g}-e_g splitting (the ellipses are still roughly half *d* character so it would have a direct effect) discussed above or, perhaps, incorporate the remaining nonspherical terms. One would really prefer to examine the issue of further adjustment on top of a general potential calculation rather than the WMT approximation used here. The approximate WMT used here is a good deal simpler and adequate to our purposes.

One should note a fairly reasonable agreement for the observed repeat distances for all three directions. Interestingly, that match occurs for the ellipse caliper with the largest m^* value: the largest phase-coherent joint density of states, i.e., phase, (in another sense) space. In Table II, the derivative of the repeat distance with shift potential is tabulated. The matching calipers also coincide with the larger derivative — or greater sensitivity, if preferred. To better appreciate these results for the ellipses, it is helpful to compare them to those resulting from a simple ellipsoidal model:

$$\varepsilon=\varepsilon_o+(\varepsilon_F-\varepsilon_o)[(k_1/0.234)^2+(k_2/0.158)^2+(k_z/0.268)^2], \tag{4}$$

where k_1 is the separation from the *N* point along (110) and k_2 is the separation along $(1\bar{1}0)$. Choosing ε_o as the calculated top of the band yields m^* values which are slightly too small but cannot affect the values of λ found. The results are tabulated in the column labeled ''Ellips.'' in Table II. Note that while this simple surface matches the initial data by construction, it yields noticeably poorer results in the (100) and (211) directions. It really does pay to consider the real band structure. On the other hand, it does also raise some

TABLE II. Kohn-anomaly repeat distances. For the three separate directions, repeat distances λ (in Å) are compared for the spanning vectors found in the unadjusted calculation ($V_\delta = 0.00$) and the adjusted calculation ($V_\delta = 0.05$ Ry). The local-joint-density-of-states strength parameter m^* is given for a single spanning vector — no multiplicity factor has been incorporated. The calipers derived from interpretation of the deHaas–vanAlphen data are listed in the column labeled dHvA [Only in the case of the ellipse $(1\bar{1}0)$ do any of these correspond to an observed multilayer repeat distance.] The results for a simple geometrical ellipsoid are tabulated in the column labeled Ellips. Also tabulated are derivatives of the repeat distance with respect to V_δ and lattice constant.

⟨100⟩	λ(0.00)	m^*(0.00)	λ(0.05)	m^*(0.05)	dHvA	Ellips.	$d\lambda/dV_\delta$	$d\lambda/da$
Ellipse (110)	13.9	0.82	16.5	0.67		15.6	8.1	17
Ellipse (011)	9.9	0.51	11.9	0.45	10.7	10.7	5.5	13
Lens (100)	30.1	0.67	37.8	0.69			13.8	53
Lens (010)	20.2	0.44	24.5	0.42			7.9	10
Lens-jack	17.7	1.19	20.7	0.91			5.0	24
Jack-jack	16.6	0.63	19.1	0.58			4.9	28
⟨211⟩	λ(0.00)	m^*(0.00)	λ(0.05)	m^*(0.05)	dHvA	Ellips.	$d\lambda/dV_\delta$	$d\lambda/da$
Ellipse (110)	11.0	0.54	13.4	0.49		12.8	6.7	19
Ellipse $(1\bar{1}0)$	15.1	0.92	17.9	0.76		16.7	8.6	19
Ellipse (011)	10.3	0.51	12.3	0.45		11.3	6.0	17
Ellipse $(0\bar{1}1)$	12.2	0.58	14.6	0.55		13.7	7.3	17
Lens (100)	27.5	0.70	34.0	0.68			10.3	40
Lens (010)	22.7	0.54	27.6	0.51			8.4	28
Lens-jack	11.9	0.53	14.5	0.32			4.6	12
Lens-jack	11.7	0.33	13.4	0.47			2.4	
Jack-jack	11.1	0.66	12.9	0.67			2.9	11
Jack-jack	10.7	0.65	12.5	0.71			2.4	12
⟨110⟩	λ(0.00)	m^*(0.00)	λ(0.05)	m^*(0.05)	dHvA	Ellips.	$d\lambda/dV_\delta$	$d\lambda/da$
Ellipse (110)	10.2	0.37	12.6	0.39	13.4	13.3	7.1	17
Ellipse $(1\bar{1}0)$	16.6	1.06	19.4	0.83	18.2	18.3	8.9	18
Ellipse (011)	11.9	0.61	14.4	0.57		12.3	7.4	18
Lens (100)	26.0	0.68	32.0	0.63			10.5	25
Lens (001)	20.6	0.50	24.9	0.46			7.2	17
Lens-jack	17.0	0.75	20.1	0.72			5.2	18
Jack-jack	16.2	0.57	18.8	0.53			4.6	22

question as to the uncertainty in the extraction of the calipers from the dHvA data, although not too severe a question since the same planes were used in that case.

Next, focusing on the lens-jack region, the *computational* improvements already result in the lens being too small — repeat distance too large — to be responsible for the long period (except for Co/Cr where the repeat distance is too large to arise from the ellipses). The *d-p* shift corrections then act to increase the difference so that the lens can be definitely ruled out as a source for the long period in the Fe/Cr multilayers. The change in this region of *k* space is more due to the much finer sampling of the Brillouin zone and the closer Fourier fit rather than to the shifts. Even though extra points were incorporated near the lens in the previous calculations,[19] this proved inadequate. Making the more careful examination for the smaller spanning vectors, calipers near the observed value do occur in the (100) and (110) directions by bridging from the lens to the jack and across the narrow neck of the jack. The situation as regards the (211) direction is less clear although, looking at the geometry, one can easily suspect that no caliper will be found in the right range.

The data to be taken from these calculations is that the empirically corrected calculation does bring the ellipse calipers in line with the experimentally observed long repeat distances; that those calipers are the large m^* ones; and that jack neck-lens structure also produces similar calipers in at least two directions.

III. ALLOYS

Alloying of the spacer material proves a very convenient probe, in no small part because the Cr-V and Cr-Mn alloys are amenable to very simple theory treatments.[27] Adequacy of alloy representation is revisited through careful comparison of a supercell calculation and the virtual crystal approximation (VCA) for a 50-50 Cr-V alloy in the bulk. Thereafter, the discussion continues using the much simpler VCA. The van Schilfgaarde–Herman (vSH) model, originally proposed in Ref. 52 and used to examine the magnetic coupling in these alloy spacer materials, is most useful to the deliberations here: the density within the layer interiors is maintained at the bulk values for the respective pure materials; only at

the interface is the electronic structure allowed to relax towards self-consistency. The vSH model was originally motivated by the efficiencies it offered. By restricting the freedom of the calculation [easily accomplished using the atomic-sphere approximation that is normally used with the linear muffin-tin orbital (LMTO) technique] inside the layers, one gains efficiency by avoiding unnecessary exploration of a lot of phase space (the ''charge sloshing''). The precision lost is partially offset by exploiting a Harris-Foulkes functional approach,[53,54] to improve the precision of the total energy — which is what is used in the analysis. The vSH model does, however, provide insufficient screening between the layers so the charge transfer effects are overemphasized. Examination of Table I of Ref. 52 indicates that this effect will not be too large for the short repeat distances (≈ 0.1 Å) but can be much more noticeable for the long repeat distances (≈ 2 Å). For our purposes, the vSH computational model provides us with a simple picture: The treatment of the layer interiors represents a linear-response approach, without the non-linear terms which are sometimes postulated to be significant. Successes of this model can give credence to the view that at least some multilayer properties do relate to bulk properties — if one can disentangle the them. (That disentangling is no small task especially when trying to use a Kohn-anomaly-type analysis as is done here. The author's own initial view of the process was that the exercise would merely present too many possibilities for any transition element. The wisdom of that early view haunts the discussion to follow.) The model does allow Fermi-level shifts, which would not normally be considered in a bulk Fermi-surface analysis. The interfaces used in the calculations are greatly oversimplified compared to the real world — a point that will reoccur often here. Nonetheless, the interface relaxation built into the model at least partially incorporates the scattering properties of the interfaces. It is reasonable to view the interface scattering calculations,[20] which suggest that *s*-*p* states are the most strongly reflected states, as a model system dissecting the interface component of the vSH model and the Kohn anomaly analysis here as a dissection of the bulk component. Alternately, the Fermi-surface analysis is precisely a parallel of a generalized susceptibility calculation with all the same issues while the focus on the surfaces is the parallel of a matrix element analysis.

The approach taken here is to examine the vSH model calculations (specifically, Fig. 2 of Ref. 27) as an ''experiment'': which must be disassembled for insight. Here, the objective is a closer look at the bulk effects. By examining the computational model, we can observe results without the extra complications of strains, defects, rough surfaces, etc. that do occur in the real experiment. This is important because it was found that surface roughness effects alone[27] were responsible for an order of magnitude difference in coupling amplitude relative to the model assuming perfect surfaces. Also the surface treatment selects a different origin for the long repeat distance in the (100) direction[55] — clearly a point to be discussed below. The computational experiment is all the more interesting since the vSH model calculations were carried out, as needs be, by calculating total energies and then fitting them to an oscillatory behavior—no Kohn-anomaly-style analysis was made other than to compare to the Fermi-surface caliper results[55] for V and Cr to assay the calipering. An alternate approach can be had at the price of using a Slater-Koster tight-binding representation for the bands. Within the limitations of that model, one can use the analytic Green's function method allowing one to focus upon the appropriate calipers with a knowledge of the associated (surface) matrix elements within a hierarchy of limiting approximations. This has been carried out for pure Cr.[21,22] A major advantage of so doing is that one gets around the difficult problem of having to obtain the repeat distances by a fitting procedure. That is a tremendous advantage since the fitting process must also account for differing decay rates and suffers from a limited range of data due to restrictions as to the largest system that can be calculated.

An overall observation should be made here. The vSH calculations found only two repeat distances to be observed except very near a transition. That only very few periods are observed even in this computational model system highlights the interesting question of why the many other Kohn singularity pairs are not observed. Scattering and surface roughness effects present in real world samples that might (further) diminish these oscillations[19] are simply not present in this computational model. This situation is quite consistent with that for Kohn anomalies in phonon spectra, where only a small fraction of Kohn singularities are actually observed. In the case of the multilayer systems, the surface introduces the matrix-element-like effects that can be characterized as reflection coefficients. These are indeed found to be strong selection factors.[56] It is easy to assume that that is the answer but is it perhaps only one factor? The differentiation between Cr and isoelectronic Mo (Ref. 57) whose repeat distance caliperings involve the same Fermi-surface pieces but in rather different combinations should provide a good probe of this issue. Further, there is the appearance that one has a selection factor, i.e., on/off, rather than just varying relative strengths. This could be due to only probing the asymptotic regime but the switch over to be seen below casts doubt on such an explanation.

Returning to the alloys, we briefly reexamine the utility of the VCA — which is not a particularly favored approximation for the description of alloy properties. That V-Cr and Cr-Mn are adjacent elements in the periodic table and are also located in the central portion of the 3*d* transition-metal series greatly favors the applicability of such a simplified treatment. Supercell results for the ordered compound, coherent-potential approximation results, and VCA results were all compared in the VSH model calculations[27] and found to yield very similar results. We can test this in a way specifically targeted to our preference for examining the system using the bcc Brillouin zone: the results of a CsCl structured ordered-alloy (supercell) calculation for CrV are compared to the virtual crystal approximation for the 50-50 alloy (i.e., setting $Z=23.5$) by ''unfolding'' them onto the bcc Brillouin zone. *Note*: one wants to ''unfold'' the bands — precisely the inverse operation to the one normally applied to estimate an ordered compound from the bands structure of a single constituent. This inverse problem is the harder one requiring some knowledge of the wave functions.

Slater-Koster[58] provide a very clear description of the relation of the simple cubic CsCl Brilloin zone to that of the larger — with twice the volume — bcc zone. The CsCl zone is carved from the bcc zone by inserting a new set of (100)

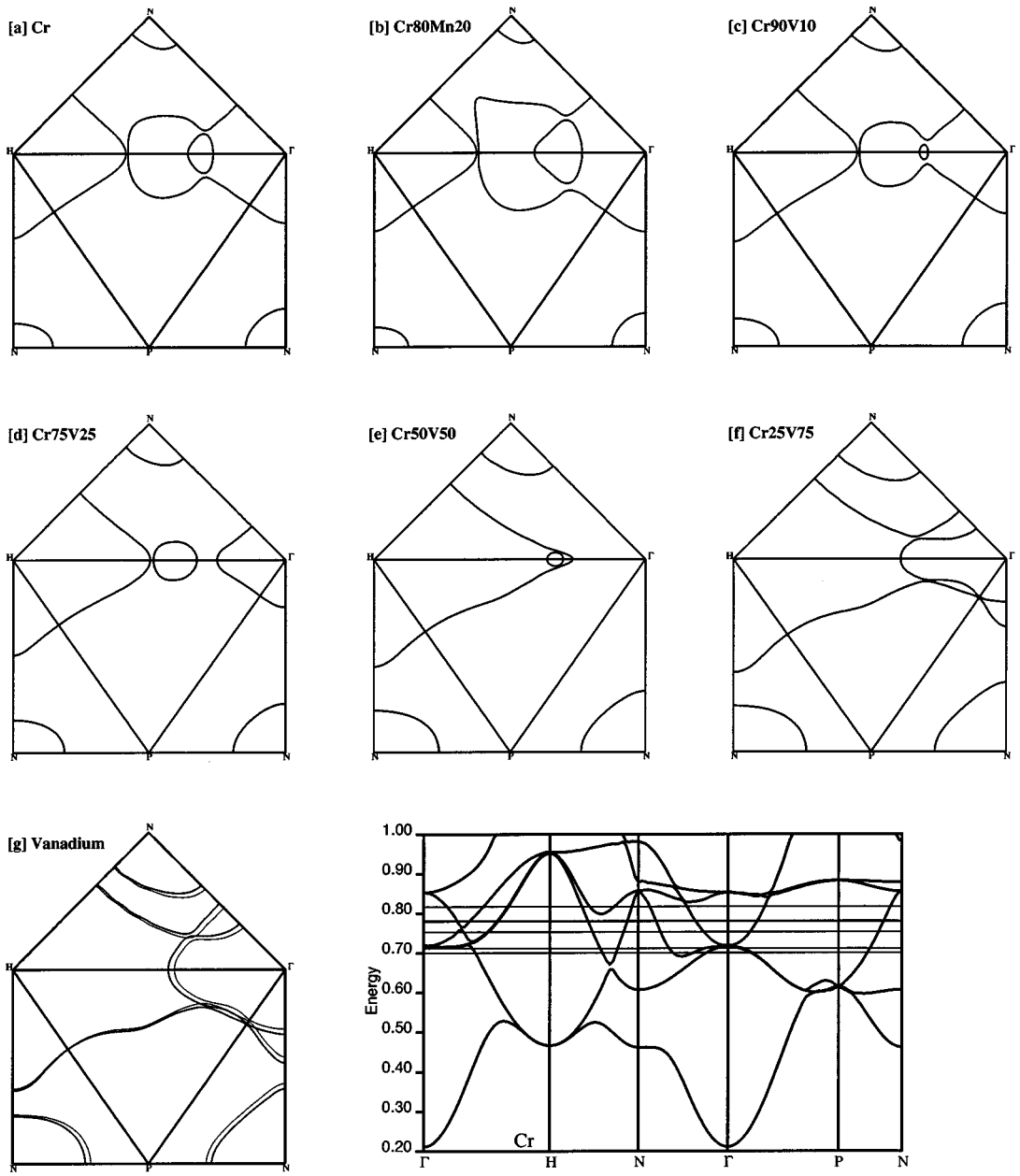

FIG. 3. The Fermi surfaces that result from the virtual crystal approximation for the range of alloy compositions from V to 30−70 Mn-Cr. In (g) for pure V, the heavier lines represent the results at the lattice constant for V and the lighter lines for the Cr lattice constant. These differences represent the changes *other than* the simple geometric lattice dilation effect. In (h), the appropriate approximate Fermi energies are shown on the Cr band structure.

planes passing through the *N* and *P* points to cut out a cube. Incidentally, these planes will pass through the ⟨100⟩ axes somewhat outside the lenses near the end of the ball on the jack. As Figs. 1 and 3 are set up, this is a true folding right down the middle line connecting *N* and *P*. The remaining volumes cut off in each direction are square-based pyramids with the *H* points for their apex. This remaining volume is mapped onto the central cube by translating each of these pyramids back using a primitive translation of the CsCl reciprocal lattice. The process maps precisely two bcc Brillouin zone points onto a single point of the CsCl zone which is the folding operation. The object here is precisely the inverse: to take the solutions at a single CsCl zone point and distribute them appropriately back onto the two corresponding bcc points. To do this, one exploits the plane-wave representation of the LAPW basis set. Given a wave-function expansion calculated for the CsCl structure, one divides the basis set of the expansion into contributions from each of the two *k* points from a bcc lattice. This is easily done precisely because we know the associated *k* for each basis function. (It could also be done for other bases sets using a projection.) One thus breaks the CsCl wave function into the sum of two basis functions coming from the two *k* points and formulates the 2×2 secular equation. What one finds is that, as long as one stays away from the CsCl zone faces, the wave function is 95% from one *k* point making the unfolding an easy process. Further, the off-diagonal terms give the scattering between the two *k*'s which directly reveals very weak scattering. It is perhaps this very weak scattering that precludes a predicted[38] exponential decay in coupling with impurity con-

TABLE III. Pseudoalloy Kohn-anomaly repeat distances for the 50-50 Cr-V Alloy. For the three separate directions, repeat distances (in Å) are tabulated for the spanning vectors on the ellipses of an ''unfolded'' CsCl structure CrV calculation. The same information is then also tabulated for a virtual crystal approximation (VCA) with $Z=23.5$. The Expt. and vSH columns are the experimentally observed period and multilayer calculated periods from Fig. 2 of Ref. 27. The Γ and ''*X*'' pocket calipers have been included as a simple indication of their size.

⟨100⟩	λ (CsCl)	*m**	λ (VCA)	*m**	Expt.	vSH
Ellipse (110)	8.0	1.69	8.1	1.58		13.7
Ellipse (011)	5.9	0.95	6.0	0.78		
⟨211⟩	λ (CsCl)	*m**	λ (VCA)	*m**	Expt.	vSH
Ellipse (110)	6.9	1.08	7.0	1.17		
Ellipse $(1\bar{1}0)$	8.7	2.26	8.6	1.34		
Ellipse (011)	6.6	0.84	6.8	1.41		
Ellipse $(0\bar{1}1)$	7.1	1.05	7.1	0.95		
⟨110⟩	λ (CsCl)	*m**	λ (VCA)	*m**	Expt.	vSH
Ellipse (110)	6.5	0.77	6.5	0.77		
Ellipse $(1\bar{1}0)$	9.4	1.82	9.4	1.32	9.6	10.2
Ellipse (011)	7.1	1.10	7.2	1.19		
Γ (band 3)	26.3	4.00	n.p.			
Γ (band 4)	32.1	0.48	n.p.			
''*X*'' pocket (011) (band 2)	56.	0.60	71	0.60		

centration although then one must ask what happens in the Ni-Cu alloys.

In Table III, the results for the VCA and supercell calculations are presented together with the observed repeat distances and the calculated vSH model results. The shift V_δ of the previous section is not incorporated into those calculations of this section which are used to compare with other calculations. None of the other calculations incorporate the adjustment. Agreement between the ordered-alloy calculation and the virtual-crystal calculation is quite remarkable. The supercell and the VCA Fermi surfaces are very similar, although the ordered compound calculation does contain two small Γ-centered pieces not present in the VCA. The compensating volume comes from within the surface around *H*—which is predominantly of *d* character—which is the explanation for the similarity of the ellipse sizes. The quite small difference between the two results that occurs does so because the *d* states at Γ are being pulled through the Fermi energy — a Lifshitz transition. Of course, very near the CsCl zone face, the splitting of the ordered supercell has been artificially eliminated consistent with a disordered material. Comparisons near that boundary would be unreasonable and we are fortunate they are not necessary.

The VCA incorporates relative shifts of the average band position in addition to the simple band filling of a rigid-band treatment. The rigid-band picture is already an excellent first picture for these materials and the band shifts further improve the reality of the description. Progressing from V to Cr, the *d* states (as measured by the simple Γ plus *H* index for their centroid) drop by about 0.5 eV. And they drop yet another 0.07 eV by addition of 30% Mn. The VCA does not, of course, incorporate any broadening effects—which can be a very significant factor when considering singularity structure as we are here. The Vegard law dependence observed for the lattice constants (i.e., linear in concentration) has been included in these calculations for Cr-V. The lattice constant has been approximated as constant (Invar-like) for the Cr-Mn alloys. The inclusion of the lattice change in the self-consistency process incorporates relaxation effects beyond the simple geometric lattice dilation incorporated in the conversion from monolayers to Ångstroms. These can be seen from a comparison of the V Fermi surface calculated at both the V and Cr lattice constants included in Fig. 3. Being plotted for a Brillouin zone scaled to the same size, the differences observed are only those other than the straightforward geometric dilation.

Across the alloy series, there are several topological Lifshitz transitions. See Fig. 3. The most pronounced transition occurs for V admixtures between 10 and 20%. It correlates well with the break in Fig. 2 of Ref. 27. It is at this concentration that the anticrossing structure along Δ in the bands is depopulated. That anticrossing structure in the bands is what connects the balls onto the vertices of the Γ-centered octahedron to produce the ''jack'' surface and simultaneously produces the lens surface within that connection. Removal of the connection between these two large pieces of surface results in a simpler structure consisting of a Γ-centered octahedron and a Δ centered ellipsoid set (much as was originally envisioned for Cr as its Fermi surface was being sorted out). A second transition occurs very near the 50% V concentration where the Γ centered octahedron is lost. Nearer pure V, the *H*-centered octahedra bridge across Γ to form the so-called jungle gym, while a Γ-centered structure is uncovered. In the opposite direction, where Mn is admixed instead of V, the famous transition to commensurate nesting occurs with dramatic effect. With further Mn admixture, the balls on

the jack surface bridge across the *N-H* lines just beyond the range of Fig. 3 between 20 and 30% Mn. In the presence of such drastic changes, it is somewhat startling that the periods found in Ref. 27 vary rather smoothly — though the same cannot be said for the amplitudes.

Although the main focus is the long periods, insight can be gained by first digressing to the short periods. In the (110) direction, the short period vascilates only slightly about 2.5 monolayers (roughly 5 Å) rising slightly towards the V end of the series. It should be remembered that this short period in the (110) direction represents a *computer experiment* since this period has not been observed. In light of the strong surface microstructure occurring for this configuration,[29,30] the prospects of actual experimental observation is poor. Although experiments with Cr-Ag spacer bilayers[59] between Co have been performed in order to examine enhanced electron-electron effects, they can also be examined to attempt to provide some evidence here. If one assumes that the coupling between the Cr and the Ag layer is only through magnitude — the surface having wiped out phase or derivative information and that the period in the Ag is extremely long (16 Å) as observed for Ag alone,[17] then the Ag layer has almost no effect on the repeat distance and the observed 5 Å repeat distance can be attributed to the Cr layer alone. Then, the 5 Å repeat distance, which is for the total bilayer thickness, must be scaled to the fractional Cr sublayer thickness (1/2.35) to get a repeat distance of 2.1 Å. As this is quite close to the monolayer separation of 2.04 Å in the (110) direction, the natural assumption is that one is seeing the basic antiferromagnetism consistent with the low temperatures employed. Of particular interest, however, is the very strong harmonic modulation also observed at a roughly two monolayer repeat distance. One must be a little careful about its interpretation. A long Ag repeat distance[17] can offer at least a partial explanation of these extreme amplitude variations within the assumed model. That size repeat distance would modulate the amplitude appearing on the Ag-Cr interface at nearly the correct rate. It would not, however, produce an effect nearly as strong as the observed variations. Subject to this concern, it is still quite reasonable to assume a superposed variation due to the couplings we are examining. This would suggest 4.2 Å repeat distances with a large error bar due to few oscillations and the superposed antiferromagnetic component. It is not a lot, but it does suggest one might be able to discover something about the (110) short period by using Ag, or other, coupling layers at the interfaces.

When attempting to compare the Kohn-anomaly analysis calculations to the results obtained from the vSH model, one is again impressed by the fact that this is indeed *not* the way one wants to do things when dealing with a complex Fermi surface: it entails long hours of searching for the reasonable result among numerous possibilities, none of which match exactly. And then one spends lots of time trying to reassure oneself that whatever is seen actually is significant. Nonetheless, a pattern does appear for the (110) short period as shown in Fig. 4: a broad band of possible calipers can be associated with the vSH result (the heavier line as read from Ref. 27) across most of the alloy range. Agreement is found for the pure element cases (V and Cr), as observed before.[27]

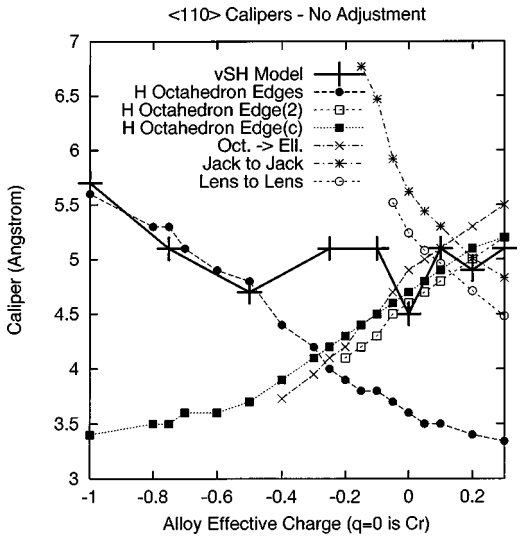

FIG. 4. Comparison of the short period found for the van Schilfgaarde–Herman (vSH) model in the (110) direction with selected Fermi-surface calipers. The results for the vSH model are indicated by the heavier curve. Data referred to in the key as ''*H* octahedron edges'' represents a caliper between the nearest edges of two adjacent octahedra. That connection remains the same as the octahedra actually bridge through the Γ point to form the jungle gym so the distinction is not made. That denoted ''*H* octahedron edge(2)'' spans a singe octahedron edge to edge along a canted diagonal near the rounding for the vertices. This ceases to be possible as the bridging occurs. Data denoted ''*H* octahedron edge(c)'' spans a single octahedron from edge center to edge center. The faces also persist when the octahedra bridge to form the jungle gym. Data denoted ''Oct.->Ell.'' couples the Γ-centered surface to the *N*-centered ellipses. This is again a jargon since only from -0.5 to -0.2 is the Γ-centered surface truly an octahedron. It then couples with the so-called *X*-centered ellipses to form the jack (and lens) surfaces. However, the octahedron like character is retained except for the (100) directions so the term octahedron is retained for the body of the jack.

Strictly as an easy index to facilitate the discussion in what follows, the alloy composition will henceforth be represented by its VCA effective charge. Define vanadium as $z=-1.0$ and Cr as $z=0.0$ so the full range runs from -1.0 to 0.3. Across the range from -1.0 to 0.5, the vSH result corresponds well with calipers arising from *H*-centered octahedron edge to neighboring *H*-centered octahedron edge. One is using sloppy language here since the octahedra actually bridge across Γ to form an open jungle gym surface in the V-rich alloys. However, the main body remains the same and the language carries the flavor so it will be used as a jargon. Actually, these points are roughly line — rather than point — singularities; which would suggest a slower $d^{-3/2}$ decay as well as the greater phase-space involvement. This apparently does not happen in the vSH calculations as their fits are consistent with a d^{-2} drop off. In the Mn alloy range from Cr (0.0) to 0.30 Mn, there is a good correspondence of the vSH model results with calipers spanning a single *H*-centered octahedron from edge to edge. Again, one is very close to a line nesting broken up by a slight variation—ether real or artifact—as can be seen in Figs. 1 and 3 from the nearly straight line on the *H* octahedron in the basal plane. In Fig. 4, two point singularities are plotted, one from center to

center (along the *H*-*N* line) and one from the point where the edge starts to turn over forming the rounded vertex. Again, if a full line nesting were to occur, one would expect a $d^{-3/2}$ decay. The correspondence is excellent except for 10% Mn where the vSH data jumps to the data denoted ''Oct.->Ell.'' That caliper stretches from the Γ-centered piece to the *N*-centered ellipse. At greater than 10% V, this Γ-centered piece is roughly an octahedron. However, in Cr and the Mn alloys, the so-called *X*-centered ellipse has been joined onto the vertices of that octahedron to form the jack surface. Since only in the (100) directions has there been a change, ''Octahedron'' is retained as a term to indicate the body of the jack. The error from inaccuracies reading the vSH model data off plots in Ref. 27 is probably at least 1/4 Å, but, if the fitting process faithfully represents a property of the vSH model — which is assumed for this discussion, then something more is happening than just the variation of the *H* octahedra and this shift should be taken as real. One possible explanation is the appearance of magnetic effects since $z=0.1$ is roughly where the vSH calculations find a commensurate *Q* vector in the (100) direction. Were this the case, one would have to understand why the effect does not continue on to higher Mn concentrations as the magnetic character continues. A more viable explanation can be constructed from available phase-space considerations. The Γ Oct.-Ell. caliper exhibits a very sharp peak precisely at 10% Mn which is so strong as to suggest a small area of nesting. It should not go unnoticed that the ellipse involves *sp* character as well. Additionally, two much smaller effective mass calipers, one from lens to lens and the other from jack-knob to jack-knob, nicely bracket the result. Although no analysis has been made of the possibility of ''mode coupling'' through the surface layer, it is appealing to consider it a possibility in this case. A positive reinforcement between the mean period of the two calipers on each side of the observed distance and the third caliper precisely at the distance could produce an enhancement. Reminding ourselves that we are in some danger of creating science fiction rather than analysis, we nonetheless note that this explanation is consistent with the wild amplitude variations seen in the vSH results which peak significantly at 10% and 30% Mn. Even with some improvement in the calculation of masses (see the Appendix), correlation between coupling strength and effective mass is weak — because other factors enter. Still, it is significant that the average masses for all three curves peak somewhere near $z=0.1$ and perhaps are even indicating nesting (line or area) tendency. This would explain the maximum at 10%, but what of the second rise at 30% Mn? It is significant there that the two octahedron spanning edge calipers [the (c) and the (2) calipers] collapse to the same distance probably indicating a long line nesting. Certainly the data from a paramagnetic calculation has done well for these magnetic systems.

The range between 30 and 10% V raises serious question. Of course, this is the range where the jack is being broken up, where amplitude for the short period in the vSH model is nearly vanishing, and where the fit is suggesting possibility of more than one short repeat distance. However, in this range there also are no calipering pairs for repeat distances anywhere near the vSH results: the vSH model results are larger while the calipers are at a minimum. (This discussion is for real space, not reciprocal space.) The Fermi surface

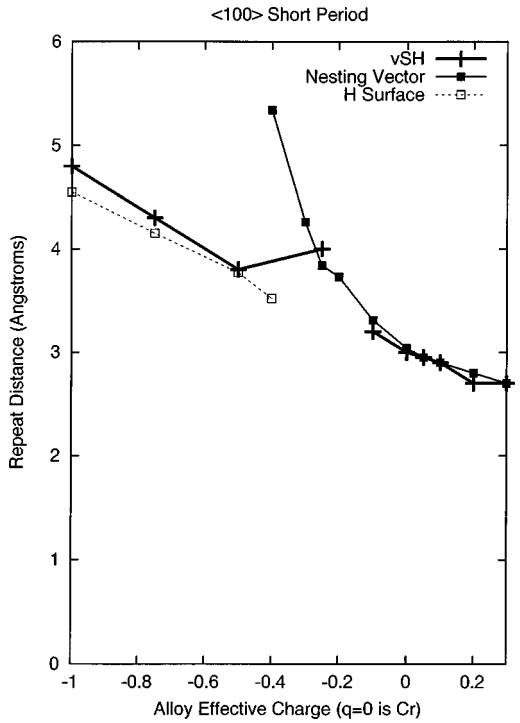

FIG. 5. The short period in the (100) direction. The van Schilfgaarde–Herman data (heaviest curve marked +) is obtained by reading their Fig. 2. The break between $z=-0.25$ and $z=-0.1$ is true to their results but the small differences seen at $z=-0.75$ and $z=0.20$ probably are not. The line marked with filled squares represents the mean nesting vector that should produce the spin-density wave in Cr. This caliper vanishes at or somewhat before $z=-0.5$ due to the depopulation of the Γ-centered surface that is at one end of this calipering. The line marked with the open squares follows a set of calipers where both ends are on the piece of surface centered at *H*, whether it be the jungle gym, which bridges across through Γ, or the octahedron that results when the bridging is closed off.

caliper distances are all significantly shorter, actually appearing nearer the harmonic of the near-neighbor antiferromagnetic repeat distance. One might argue that the variation is hard to detect on the original plots from which the data was taken and that the amplitude is strongly suppressed there. However, although the error bars are admittedly large, the optical scanning does give some resolution and, most significant, it is clear that the two data points rise above a smooth curve, while the Fermi surface calipers would fall below. This small feature, much exaggerated in Fig. 4, does have a reasonable probability of being reality.

The short repeat distance for the (100) direction is shown in Fig. 5. This case appears somewhat simpler. The vSH results very explicitly exhibit the break between $z=-0.25$ and $z=-0.1$ that has been mentioned above. The alloy regime from 10 V to 30% is quite simple. Excellent agreement is seen to exist in this regime between the vSH curve and the curve of the mean nesting vector spanning from the *H*-centered octahedron to the Γ-centered part (body) of the jack. (As above, this piece that forms the main body of the jack is identified using the name Γ-centered octahedron. This is reasonable since the surface remaining after the Fermi energy has sunk below the bridging energy is precisely a

Γ-centered octahedron.) It is, of course, this nesting vector that is associated with the spin-density wave. In both the calculations for the vSH model and those here, that nesting vector becomes coherent at 10% Mn. It occurs sooner at about 5% experimentally, but that is in part due to pulling or lock-in effects.[60–62] Nothing is to be made of the small difference at $z=-0.2$ because it appears to be an interpolation error not reflected in the original figure. The nesting vector curve does continue on below $z=-0.1$ down to around $z=-0.5$ where the Γ-centered piece becomes fully depopulated. It is still very strong at $z=-0.25$ where it would appear to again agree well with the vSH results. At $z=-0.3$, it begins to broaden — wider range of spanning vectors about the mean — and to weaken: i.e., fewer calipers found each with significantly smaller masses. In the regime from $z=-1.0$ (V) to $z=-0.5$, the vSH results agree very well with a different set of calipers that involve the *H*-centered piece (as jungle gym or octahedron) at both ends. These *H*-*H* calipers exhibit a strong local joint density of states, being multiply occurring with high mass values actually hinting of a possible nesting, near the V-rich side, but become of negligible strength beyond $z>-0.4$ where the calipering jumps to a single point of significantly shorter repeat distance and low mass. Obviously, such an analysis cannot be expected to tell us much about the switch over occurring between $z=-0.5$ and $z=-0.25$. It does, however, suggest a closer look at this region might prove interesting. Further, the fact that the vSH model gives a point on the Γ-*H* nesting curve beyond the gap indicates an important puzzle: There is nothing in the Kohn-anomaly analysis that would suggest the gap should occur. That it might be an earlier switch over is denied by the existence of that point beyond the gap. It is perhaps possible that, as the Fermi-surface breakup occurs, the transitioning *k*-space regime generated around the critical point produces greatly increased scattering from the states on the faces of the Γ octahedron.

Ending the digression to the short periods, focus returns to the long periods. In the (110) direction, initial presumption is that the long periods arise from the *N*-centered ellipses. A comparison of the results for the vSH model and the three Kohn-anomaly calipers is shown in Fig. 6. Although the (real) experimental data is presented there as well, its consideration is delayed until considering the results incorporating the empirical shifts while first continuing the computational experiment without them. For $z>-0.5$ the vSH results and the zone surface caliper occurring along the *H*-*N* line across the ellipse agree reasonably well. The difference observed is somewhat larger than the difference obtained when comparing bulk APW and bulk LMTO calculations which suggests another small effect is present. Greater deviation occurs above $z=0.1$, which is only mentioned but not discussed here. The zone face ellipse caliper appears to correspond to the vSH model all across the alloy series. Of the other two *N*-ellipse calipers, the ''straight-out'' vector along the Γ-*N* line is too small in real space, meaning too large in reciprocal space, to be a possible factor in the response. The same is mostly true for the ''canted'' vector (the one that does not occur in the basal plane) except for alloy compositions near the V-rich end.

Comparison of the empirically corrected calculations to the real experimental data, shown in Fig. 7, reveals something new and quite interesting. In the alloy range from about 50-50 V/Cr to pure Cr, the experimental data coincides well with the zone surface caliper along the *H*-*N* line through the ellipse. But, beyond 50% V, it *switches* to agree well with the ''canted'' caliper (one in the ⟨101⟩ direction for an ellipse along the ⟨110⟩ direction). This result causes regret that there are no data between 50 and 75% V. The same switch does not occur in the vSH model — at least not with the simplest version of the interface. The calculated caliper effective mass parameters do cross over near $z\approx-0.7$ with the canted vector caliper having the largest mass on the V-rich side where it is apparently being seen. Note that apparently only one or the other caliper is being observed, not a combination with varying amplitudes. And that this is occurring where the strengths of the two channels must be very nearly equal — the most favorable case to see both contributions.

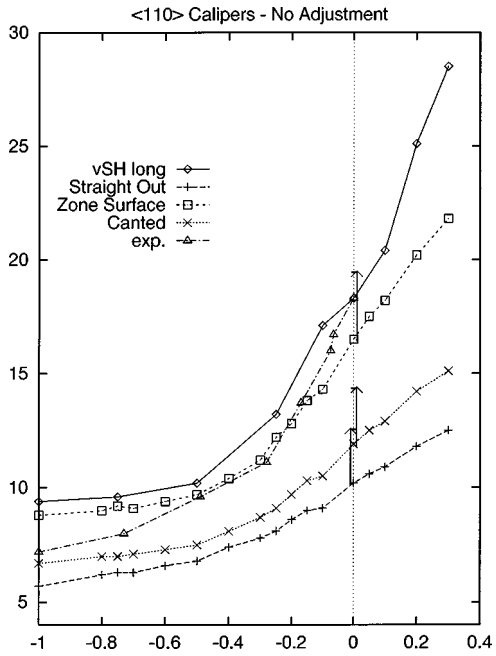

FIG. 6. Comparison of the vSH model results with ellipse calipers for the long period in the (110) direction. Labels used in the key indicate the following: vSH long and exp. indicate the results of the vSH model and experimental results as read from Ref. 27; Straight Out indicate the ellipse caliper along the Γ-*N* line; Zone Surface is the ellipse caliper along the *H*-*N* line; Canted is the one caliper that extends out of the basal plane. Calipers were calculated without the adjustment of the previous section for comparison with the vSH model calculations. The arrows at $z=0.0$ illustrate the effects of the adjustment, which is incorporated in Fig. 7 for comparison with actual experiment.

The most complicated situation occurs for the (100) long period results shown in Fig. 8. A conclusion quickly drawn from this figure is that the vSH results have very little to do with calipers on the ellipses. The sole weakly credible exception is at $z=-0.25$ where the ellipse caliper in the basal plane is the closest caliper to the vSH curve. (The closest caliper on the upper side is a coupling between the Γ centered octahedron and an ellipse. It is marked by a small asterisk. Neither can be considered reasonably close.) In the V-rich region, the vSH results are closely represented by a caliper pair coupling an ellipse to the body of the *H*-centered surface. It is the interconnected jungle gym at V converting

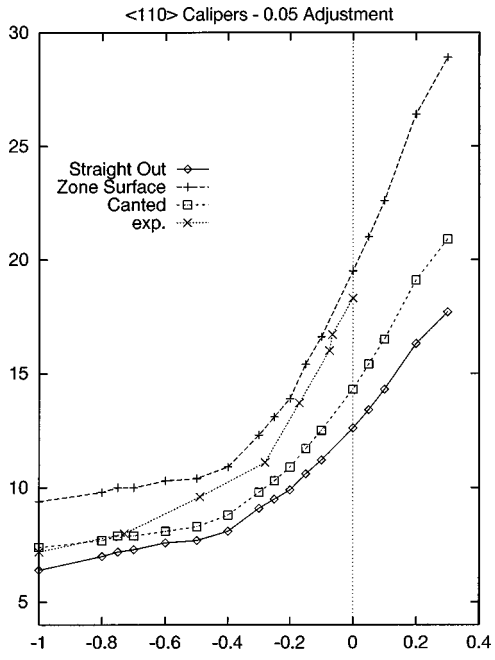

FIG. 7. Comparison of experimental results with the ellipse calipers for the long period in the (110) direction. Key labels are the same as in Fig. 6. Note that the experimental data apparently switches from matching with the zone face caliper to matching the canted vector caliper near the V-rich end.

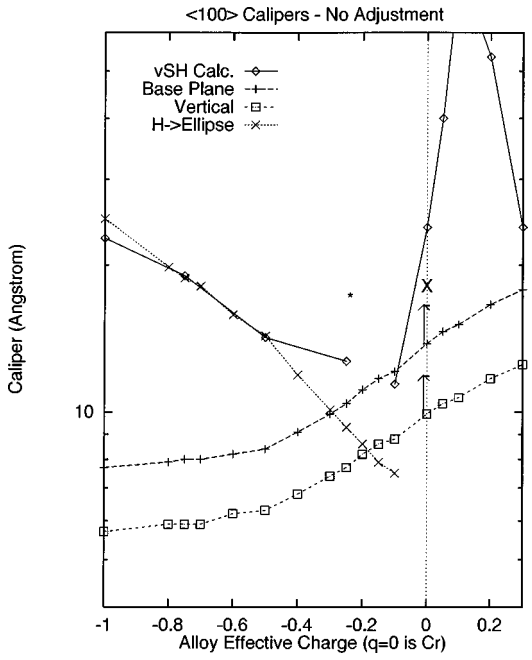

FIG. 8. Comparison of the vSH model results with selected calipers for the long period in the (100) direction. Key labels indicate the following: vSH Calc. is the results of the vSH model for the long period; Base Plane is the ellipse caliper occurring in the basal plane (two are equal by symmetry); Vertical is the ellipse caliper perpendicular to the basal plane; *H->*ellipse is a caliper between the surface centered at the *H* point and an ellipse. The sole experimental data point is indicated by a large *X* for Cr. The arrows give the same information as in Fig. 6.

to a closed piece roughly at the 50% alloy composition. (Refer to Fig. 3.) On the other side of the break, the dramatic singular curve seen for the vSH model in the Cr-Mn alloys arises from the same nesting as the short period. The reduced symmetry of the slab, or aliasing due to discrete sampling, produces an effective repeat vector (in reciprocal space) which is the difference from $2\pi/a$ of the short period vector. The long period vector goes through zero as the material becomes commensurate (short vector goes through $2\pi/a$) so the repeat distance, which is the reciprocal, diverges. This result, correct for the vSH model calculation, does not represent the experimental situation. But it is clearly reflected in the Fermi-surface calipering. So this part of the computer experiment does not give further information.

Examining the cause is more interesting. Part of the answer can be gleaned from studies examining the effects of surface roughness. In a computational experiment to determine sensitivity to interface roughness,[27] a checkerboard pattern of Cr and Fe was created at the interface. The resulting effect was that the amplitudes of both the long and the short period were reduced by very similar factors (5.8 and 6.1): actually a significant improvement to the order-of-magnitude theoretical overestimate for the amplitude found using the perfect interface. Experimentally, however, the long period persists even for quite rough interfaces. So the precipitous diminution of the long period is not consistent with the experimental findings and is just one more piece of evidence that the nesting alias is not the origin of the long period.

Instead, model calculations for interface reflection properties[20] indicate that the Fe layers used in the vSH model calculation were too thin: Fe layers only two monolayer thick were used. (One would like to view the reflection calculations as doing a similar decomposition for the interface component of the problem to what is done by caliper calculations for the bulk response.) Thicker Fe layers are needed to achieve strong reflection for the calipers on the *N* ellipses, a not surprising result because of the *p* character admixture in the wave functions for the states on that surface. Tight-binding calculations specifically studying effects due to the degree of confinement[63] find that the amplitude (and phase) are dramatically affected, but not the repeat distance by interface roughness. Actually, the repeat distance can be changed, but through selection of a different caliper. Modification of relative amplitudes by changes in the magnetic layer thickness has also been seen for (Co/Cu) multilayers.[64] In that case, the variation in thickness actually changed which of two differing experimental results were matched by the theoretical calculations. The explanation tendered involved the differing sample preparations.

Further confirmation that the root cause for the vSH result is the thinness of the Fe layer can be gotten from calculations[23] for a model quite similar to the vSH model — being based on LMTO calculations with subsequent fits to variation of the total-energy difference (between ferro- and antiferromagnetic alignment of the layers) to extract repeat distances — but with two major differences: retaining full self-consistency in the spacer layer; and utilizing semi-infinite Fe slabs. The self-consistent response appears to affect the repeat distances very little, indicating a minimal effect of the incipient, or present, antiferromagnetism. Of primary interest to the present consideration is that the semi-infinite Fe slabs eliminate the appearance of the nesting alias as the short period. A short period of 2.07 monolayers

(=2.98 Å) is found which decays as $1/d$ consistent with a nested surface. A long period of 11.98 monolayers (=17.2 Å) is also found which decays as $1/d^2$ consistent with a point calipering. Found in addition are two very rapidly decaying terms. The long period, however, is interpreted not as arising from the *N*-centered ellipses but from an unusual coupling between *H* octahedra. It is argued that enough persists of the Cr antiferromagnetic character for the system to be analyzed using a CsCl unit cell. In that structure, the octahedra would be folded in to the Γ point. One could then get a corner to corner (of the octahedron in the next zone) transition which comes out to be just the correct size. Present calculations yield a repeat distance of 16.4 Å for such a ''CsCl caliper'' when the empirical adjustment is not applied and 17.4 Å when it is. Most likely the reason that the correspondence is to the adjusted calculation is that the atomic-sphere shape approximation is simulating the effect. The effective mass for this calipering is fairly small—being about a half—and the coupling is *d* to *d* so this interpretation is subject to all the criticism applied to a lens/jack-type interaction. Such an interpretation also would encounter problems when examining the $\langle 211 \rangle$ direction. But more seriously, such an explanation would prove inconsistent with the V-alloy behavior for the (100) direction. At 10% V, the repeat distance due to such a calipering *increases* to 30 Å whereas the experimental result[65] *actually decreases*. Also, photoemission ''sees'' no evidence of quantum-well states forming along the direct (100) direction. It thus seems unlikely that this interaction occurs in the real world, although it apparently does exist within the model. It is important to take note that the interpretation of this calculation does not point to an ellipse caliper. Whether it might exist in the calculation is not clear because an ellipse caliper is not given. (As an aside, the observation can be made that the concerns of Mirbt *et al.*[23] about the possible appearance of a bcc caliper $\tilde{Q}_4$ from the lens to the jack-knob/octahedron-tip is unfounded. That caliper would have to arise not from the *H* side of the lens but from the Γ side in order for the velocities to be antiparallel. In that case, the repeat distance would be far too short (about 9 Å) to be considered as a candidate for the long period.)

One learns somewhat more about the short period amplitude from Ref. 23. The amplitude obtained is larger than experiment by *three* orders of magnitude compared to the single order of magnitude found for the vSH model. A significant part of this effect could be the greater effective confinement, so one cannot simply point to the greater response incorporated in the bulk without more careful consideration. It is certainly suggestive, though, since this oscillation involves only *d* states and so should not require thick Fe layers. In this model, even more is required from surface roughness to bring the calculated amplitude down to what is observed experimentally.

Several observations should be taken from this section. The primary result is that reasonable identification of calipers can be found throughout almost all of the alloy range. This makes the exceptions much more interesting although they are usually found at places of transition with small amplitudes. For the long period in the $\langle 110 \rangle$ direction in the V-rich alloys and in the $\langle 100 \rangle$ direction generally, calipers can be successfully associated with the vSH model results and with the experimental results but they are different. In the $\langle 100 \rangle$ direction, this is attributed to using Fe layers that were too thin in the calculations for the vSH model. Another observation to be taken concerns possible intermode coupling. In the analysis for the short period in the $\langle 110 \rangle$ direction of the Mn alloys, it was suggested that one possible explanation would involve several calipers acting in concert. That suggestion would seem at odds with a more general behavior involving switching between modes, as apparently seen relative to the *H* octahedron calipers and also for the long period in this same direction for the V-rich alloys, for an example.

IV. MORE SURFACE EFFECTS

Motivated by the lack of corresponding Fermi-surface calipers for the short period in the (110) direction at around 20–25% V, the analysis of Mirbt *et al.*[23] can be examined a bit further. It can be extended under a somewhat different view which will prove instructive but not resolve the issue. Instead of focusing on the spin-density-wave character, it is useful to instead reconsider the fact that the Cr-Fe interfaces lower the symmetry of the system. For interfaces perpendicular to the $\langle 100 \rangle$ direction, a symmetry lowering is introduced that would be properly represented by analyzing the problem using a CsCl-type lattice. That would not, however, be the case for other directions. Rigorously, once the interfaces have been introduced, one no longer has periodic boundary conditions in the normal direction and no proper reciprocal space in that direction. For large enough spacer material and ''reasonable'' interfaces, one can get by in the analysis simply continuing as though all was in order. Such is the nature of most of the the Fermi-surface singularity analysis being utilized here. So one knows that one can at least ''almost get by'' and the natural question is what will be the first effect(s) to appear next. Most reasonable is that all 2D reciprocal-lattice vectors of the interface plane should start to appear. Generally, the plane is more open than the bulk solid so this will introduce reciprocal lattice vectors which are some fraction of the bulk reciprocal-lattice vectors. See Sec. II B of Ref. 19 for a discussion. This will introduce a very specific new coupling within the Brillouin zone because the interfaces truncate the summation (implied by the discussion of a generalized RKKY formalism[66] that brings in the reciprocal-lattice vectors) precluding obtaining the full bulk crystal orthogonality. Another way to get to this result is to realize that a supercell treatment for the ideal system would result in a wafer-thin Brillouin zone based on the plane 2D zone. If one then assumes one can do an unfolding like that used to test the VCA above, then the first new effect is the presence of the plane vectors. Accordingly, one can look for a new set of spanning vectors *except* that the two Fermi-surface spots associated with a repeat vector *q* are also displaced by a reciprocal-lattice vector of the interface.

The ideas are easiest to see by considering the the original case where the interfaces have a (100) normal. In this case, the planes are simple square lattices which stack with each plane above the square center of the adjacent plane. The 2D primitive translations are $(0a0)$ and $(00a)$ with the associated reciprocal-lattice vectors are $2\pi(010)/a$ and $2\pi(001)/a$. (Clearly, the normal is in the *x* direction.) These

are the extra vectors in the perpendicular direction for a CsCl Brillouin zone to apply. These are the only directions needed for the effect observed. However, in the (100) direction, aliasing or coupling with one of the bulk reciprocal-lattice vectors will produce a comparable effect. Hence, the interfaces do introduce the use of a CsCl Brillouin zone and are at least as probable a basis as the explanation used.[23]

When the interface normal is in the (110) direction, the planes are face-centered rectangular 2D lattices which are stacked above edge centers. Using the 3D vectors, the primitive translations of the planes are $a(1,-1,1)/2$ and $a(1,-1,-1)/2$ and the reciprocal-lattice vectors are $\pi(1,-1,2)/a$ and $\pi(1,-1,-2)$. The main effect of incorporating the surface-derived displacement vectors is to give an out-of-plane *H*-centered octahedron a virtual position allowing it to interact in the (110) direction with the ellipse and a basal plane *H* octahedron. The major result was an interoctahedron caliper at 2.1 Å and an ellipse-octahedron/interoctahedron caliper at 6.2 Å. There does not appear to be anything closer to the vSH model result of 5.1 Å than the 6.2 Å which merely brackets the value on the high side by an about equal amount to what had been found on the low side using standard calipering.

Note that this simple extension does not introduce a $2\pi(001)/a$-type vector for the (110) direction unless something acts to remove the face centering in the plane. (Or, one could return to the magnetic response arguments . . .) However, if a $2\pi(001)/a$ vector is assumed to be present, then (110) caliperings are introduced between the *H* octahedra and between the Γ and *H* octahedra. One of these calipers between the Γ octahedron and an *H* octahedron has a repeat distance of 4.9 Å and effective mass parameter of 2.2. So these two somewhat questionable results prove illusive within the models examined here.

V. DISCUSSION

The results presented have discredited several of the hypotheses under which this study was begun, and also focused several additional issues. By matching the size of the *N* ellipses to that inferred from dHvA data, through an empirical correction of the *d*-band energy, one indeed finds that Fermi-surface caliperings can be found on the ellipses[20–22] appropriate to the long period. This is clearly much better than the previous situation where only very special cases could be found. It is also not a trivial result since the ellipse data is actually derived information from the actual experiment: it must be backed out from the data by working around the effects of the spin-density wave. The data provided is then the principal axis dimensions of an assumed ellipsoidal surface. It was shown that the ellipsoidal assumption is deficient for the purposes here although probably adequate to the original extraction. For the (100) direction, the primary caliper arises from the basal plane (as found previously). This caliper does have the higher mass factor of the 2 occurring on the ellipse, as does the zone-face caliper appropriate for the (110) direction. This selection among the subset of ellipse calipers is only slightly further emphasized by the higher spin antisymmetric reflection factors[21,22] representing the surface effects.

Improved calculations yield a lens surface which is too small for the long repeat distance, and increases the anisotropy, thereby adding more evidence against the hypothesis that it might be the responsible surface. The empirical correction of the *d*-band energy then only acts to increase the difference. At the same time, the caliper across the neck of the Γ-centered jack surface comes to be nearly the correct size and the caliper from the lens to the jack neck becomes the correct size for Co/Cr multilayers — where the ellipses apparently do not fit. So, for the (100) direction, one has the at least three other features of the right size: jack neck, alias of the short period, and coupling of the *H* octahedron in a CsCl structure. The fact that the jack neck caliper is seen in photoemission[26] coupled with the question of why the long period is so robust suggests that one might ask whether these additional channels might not couple into the response to enhance it. The first evidence that this may not be the case actually comes from the fact that the amplitude and repeat distance are essentially identical for both the (100) and the (211) direction. The (211) direction is geometrically much more complex but it does not appear other possible channels are to be found there — raising serious doubts about such a hypothesis. Much stronger evidence comes from the computer experiment on the Cr/(V,Mn) alloys. In the one case where it might be tempting to appeal to mode coupling enhancement [short period in the (110) direction for 10% Mn], it is actually much more dramatic that that result occurs because of a mode exclusion. And there are quite a few cases where one sees mode *switching* as a function of alloy composition which would naturally suggest a predilection for mode exclusion. Understanding such an exclusion would be very useful to explain why there are so many more Fermi-surface calipers than actual terms in the response: it is improbable that simple amplitude arguments are enough.

And what of the robust character exhibited by the long period? Is it a magnetic enhancement effect? Certainly comparison of the amplitudes found with[23] and without[27] enhancement find a huge difference for the short period. Perhaps this really does extend to the long period but it still needs checking since that is a piece of Fermi surface with very different wave function character.

ACKNOWLEDGMENTS

This work was supported by the U.S. Department of Energy, Basic Energy Sciences, Division of Materials Sciences under Contract No. W-31-109-ENG-38 and by a grant of computer resources and the National Energy Research Supercomputer Center. The author is grateful to Greg McMullan for performing the series of LMTO calculations that permitted a detailed comparison of the results obtained by the two different approaches.

APPENDIX: FURTHER MINOR IMPROVEMENT ON THE MASS (LOCAL JOINT DENSITY OF STATES) EXPRESSION

The local joint density of states, or mass parameter, has proven a poor criterion for the strength of any particular Fermi-surface caliper pair because of the other factors involved. A minor further improvement will be presented here

which has an effect on the mass parameter calculated for some caliper pairs.

The mass parameter is defined assuming a point extremum or saddle point.[15,67,68] When there is actual nesting along a line [as for the *H*-centered octahedron in the basal plane for a (110) vector] the definition of the mass parameter diverges. When this happens, the joint density of states involved is much greater and the strength of the coupling falls off as $d^{-3/2}$. When the nesting occurs for a full plane (the classic Γ-centered jack to *H*-centered octahedron associated with the Cr spin-density wave, for example), the joint density of states is even stronger and the strength of the coupling falls off as d^{-1}. It is an unfortunate feature of the Fourier series (star) function fitting technology used that line or area nesting is not found directly. Because the fit contains small nonphysical oscillations—remnants of Gibbs ringing, the fit always exhibits point calipers. Nesting is then detected by multiple calipers of differing type and high mass that occur closely spaced in the same region. These require manual identification by careful examination of the results. But they are important to identify because extending nesting is so more significant than point calipering. It is most likely that these small improvements in the determination of the mass parameter have, as their most useful consequence, helping to spot in spotting nesting.

With the above proviso, improvement can be made even on the slightly improved version of Ref. 19. That notation will be followed here due to familiarity. We return to the expression for the intensity

$$I=\frac{-Z}{2(2\pi)^4}\int d^2\vec{k}_\parallel\int dk_z\int dk_z' e^{iz(k_z'-k_z)}\frac{f(\varepsilon)-f(\varepsilon')}{\varepsilon-\varepsilon'}. \tag{A1}$$

In this expression, the factor Z is an approximate matrix element which is assumed slowly varying — the arguments expressing its dependence on the two calipering vectors have merely been suppressed for clarity. That dependence, though important, is not the focus here. (It is where the often very important surface interactions are buried.) Only one $\vec{k}_\parallel$ integration appears because a two-dimensional δ function has already been evaluated. The f's are Fermi occupation-number functions. For simplicity of notation, the presence or nonpresence of a prime on the ε is used to associate it with the appropriate k vector and band index arguments. The procedure to evaluate the k_z integrals is to convert them to energy integrals using a linearized (in k_z) quadratic expansion about the calipering vectors. This is straightforwardly accomplished so long as a linear relation is an adequate approximation over the thin region where $f(\varepsilon)-f(\varepsilon')$ has a significant value. The energy integrals can be evaluated by continuing into the complex plane and summing the residues. Moving to the caliper vectors as an origin, the exponential contains an overall phase factor dependent on the spanning vector (the difference between the two calipering vectors) which can merely be moved out in front of the integrals. One now works with the quadratic expansion for both vectors (the primes are inserted when needed):

$$\varepsilon=\vec{v}\cdot\vec{k}+\frac{1}{2}\vec{k}\cdot\overleftrightarrow{D}\cdot\vec{k}. \tag{A2}$$

The quadratic matrix is constructed to be symmetric. This expression is rotated to an orientation along the spanning vector (k_z) and the two-dimensional vector perpendicular to it, identified as the vector ''parallel'' to the surface ($\vec{k}_\parallel$):

$$\varepsilon=\vec{v}\cdot\vec{k}_\parallel+\frac{1}{2}\vec{k}_\parallel\cdot\overleftrightarrow{D}\cdot\vec{k}_\parallel+k_z(v_z+\hat{z}\cdot\overleftrightarrow{D}\cdot\vec{k}_\parallel)+\frac{1}{2}D_{zz}k_z{}^2. \tag{A3}$$

If the $D_{zz}k_z{}^2$ term can be neglected—one type of ''thin Fermi shell,'' then one has an easy, approximate inversion:

$$\tilde{k}_z\approx\frac{\varepsilon-\vec{v}\cdot\vec{k}_\parallel-\vec{k}_\parallel\cdot\overleftrightarrow{D}\cdot\vec{k}_\parallel/2}{v_z+\hat{z}\cdot\overleftrightarrow{D}\cdot\vec{k}_\parallel}$$
$$\approx\frac{1}{v_z}\left(\varepsilon-\vec{v}\cdot\vec{k}_\parallel-\vec{k}_\parallel\cdot\overleftrightarrow{D}\cdot\vec{k}_\parallel/2-\frac{1}{v_z}\hat{z}\cdot\overleftrightarrow{D}\cdot\vec{k}_\parallel\right). \tag{A4}$$

This is the expression used in Ref. 19. One can improve on this by making a linear expansion about $\tilde{k}_z$:

$$k_z{}^2\approx\tilde{k}_z{}^2+2\tilde{k}_z(k_z-\tilde{k}_z)=\tilde{k}_z(2k_z-\tilde{k}_z). \tag{A5}$$

Reinserting this approximation retains a linear solution in k_z and permits an improved approximation

$$k_z\approx\frac{\varepsilon-\vec{v}\cdot\vec{k}_\parallel-\vec{k}_\parallel\cdot\overleftrightarrow{D}\cdot\vec{k}_\parallel/2+\tilde{k}_z{}^2D_{zz}/2}{v_z+\hat{z}\cdot\overleftrightarrow{D}\cdot\vec{k}_\parallel+D_{zz}\tilde{k}_z}, \tag{A6}$$

which, however, is not linear in ε because of the $\tilde{k}_z$ in the denominator and its square in the numerator. This nonlinearity in ε would preclude the straightforward contour integration technique used for ε and ε'. However, because those integrations result only in the slowly varying $(z/L)/\sinh(z/L)$ term, this change would not be an important correction and is ignored. What is important is the correction to the $\varepsilon=0$ surface associated with the steepest descent $\vec{k}_\parallel$ integral. What is being done then is to modify the curvatures of the approximate Fermi surfaces used in the steepest descent integral. For that, one sets ε to zero and expands the k_z and k_z' expressions to obtain the required quadratic expression used in the steepest descent. The result can be achieved by a simpler and more transparent approach if one notes that, to the level of expansion being utilized, the $\tilde{k}_z$ associated with the quadratic term reduces to the simple tangent term

$$\tilde{k}_z\rightarrow-(\vec{v}\cdot\vec{k}_\parallel/v_z). \tag{A7}$$

Thus, one can evaluate the quadratic term for the vector

$$\vec{k}_o=[\vec{k}_\parallel,-(\vec{v}\cdot\vec{k}_\parallel/v_z)] \tag{A8}$$

in the $\varepsilon=0$ expression and solve:

$$k_z=\frac{1}{v_z}\left(-\vec{v}\cdot\vec{k}_\parallel-\frac{1}{2}\vec{k}_o\cdot\overleftrightarrow{D}\cdot\vec{k}_o\right). \tag{A9}$$

Since the velocities at the two calipering vectors are antiparallel, the linear term will cancel out. Because of the tangent relation, all terms in the bilinear product contain precisely two factors of $\vec{k}_\parallel$ so it can be rewritten as a bilinear product of $\vec{k}_\parallel$ and a rotation performed to achieve a diagonal tensor.

The resulting diagonal matrix elements are the inverse of the mass elements needed for the local joint density of states expression. This is believed to be about the best one can do within the limits of the integration techniques used. One can go somewhat farther using alternate techniques to deal with the integrations and even analytically examine weak nesting[69] by incorporating the next terms in the expansion when the second-order terms are zero. These nesting effects are very important but, as noted above, the expansions used do not permit direct evaluation without very elaborate efforts. While generally less precise, the tight-binding representation[20] does provide a more direct indication of nesting because it does not contain the short-wavelength oscillations.

[1] P. Grünberg *et al.*, Phys. Rev. Lett. **57**, 2442 (1986).
[2] S. F. Alvarado and C. Carbone, Physica B **149**, 43 (1988).
[3] M. Baibich *et al.*, Phys. Rev. Lett. **61**, 2472 (1988).
[4] J. Krebs, R. Lubitz, A. Chaiken, and G. Prinz, Phys. Rev. Lett. **63**, 1645 (1989).
[5] S. Parkin, N. More, and K. Roche, Phys. Rev. Lett. **64**, 2304 (1990).
[6] A. Davies, J. A. Stroscio, D. Pierce, and R. Celota, Phys. Rev. Lett. **76**, 4175 (1996).
[7] D. Stoeffler and F. Gautier, Phys. Rev. B **44**, 10 389 (1991).
[8] D. Stoeffler and F. Gautier, J. Magn. Magn. Mater. **104-107**, 1819 (1992).
[9] J. Unguris, R. Celotta, and D. Pierce, Phys. Rev. Lett. **67**, 140 (1991).
[10] J. Wolf *et al.*, J. Magn. Magn. Mater. **121**, 253 (1993).
[11] Y. Wang, P. Levy, and J. Fry, Phys. Rev. Lett. **65**, 2732 (1993).
[12] Z.-P. Shi, P. M. Levy, and J. L. Fry, Phys. Rev. Lett. **69**, 3678 (1992).
[13] P. M. Levy *et al.*, J. Magn. Magn. Mater. **121**, 357 (1993).
[14] S. Parkin, Phys. Rev. Lett. **67**, 3598 (1991).
[15] P. Bruno and C. Chappert, Phys. Rev. B **46**, 261 (1992).
[16] P. Bruno, J. Magn. Magn. Mater. **116**, L13 (1992).
[17] S. Araki, J. Appl. Phys. **73**, 3910 (1993).
[18] M. van Schilfgaarde and W. A. Harrison, Phys. Rev. Lett. **71**, 3870 (1993).
[19] D. D. Koelling, Phys. Rev. B **50**, 273 (1994).
[20] M. D. Stiles, Phys. Rev. B **54**, 14 679 (1996).
[21] L. Tsetseris, B. Lee, and Y.-C. Chang, Phys. Rev. B **55**, R11 586 (1997).
[22] L. Tsetseris, B. Lee, and Y.-C. Chang, Phys. Rev. B **56**, R11 392 (1997).
[23] S. Mirbt, A. M. N. Niklasson, B. Johansson, and H. L. Skriver, Phys. Rev. B **54**, 6382 (1996).
[24] P. Bruno, J. Magn. Magn. Mater. **121**, 248 (1993).
[25] E. E. Fullerton *et al.*, Phys. Rev. B **48**, 15 755 (1993).
[26] D. Li *et al.*, Phys. Rev. Lett. **78**, 1154 (1997).
[27] M. van Schilfgaarde, F. Herman, S. S. P. Parkin, and J. Kudrnovský, Phys. Rev. Lett. **74**, 4063 (1995).
[28] E. E. Fullerton, the Cr periods in the (100) and (211) directions differ by less than 6% (unpublished).
[29] W. Folkerts and F. Hakkens, J. Appl. Phys. **73**, 3922 (1993).
[30] A. Kamijo, J. Magn. Magn. Mater. **156**, 137 (1996).
[31] J. E. Graebner and J. A. Marcus, Phys. Rev. **175**, 659 (1968).
[32] G. W. Crabtree, D. Dye, D. P. Karim, and D. D. Koelling, Phys. Rev. Lett. **42**, 390 (1979).
[33] G. W. Crabtree *et al.*, Phys. Rev. B **35**, 1728 (1987).
[34] R. Blaschke *et al.*, J. Phys. F **14**, 175 (1984).
[35] V. I. Anisimov, F. Aryasetiawan, and A. I. Lichtenstein, J. Phys.: Condens. Matter **9**, 767 (1997).
[36] S. Wakoh and J. Yamashita, J. Phys. Soc. Jpn. **35**, 1394 (1973).
[37] J. Mathon, M. Villeret, and D. Edwards, J. Phys.: Condens. Matter **4**, 9873 (1992).
[38] J. d'Albuquerque e Castro, M. Ferreira, and R. Muniz, Phys. Rev. B **49**, R16 062 (1994).
[39] J. Mathon *et al.*, Phys. Rev. B **56**, 11 797 (1997).
[40] S. Wakoh, Y. Kubo, and J. Yamashita, J. Phys. Soc. Jpn. **38**, 416 (1975).
[41] S. Wakoh, Y. Kubo, and J. Yamashita, J. Phys. Soc. Jpn. **40**, 1043 (1976).
[42] S. Wakoh and Y. Kubo, J. Phys. F **10**, 2702 (1980).
[43] N. Shiotani *et al.*, J. Phys. Soc. Jpn. **43**, 1229 (1977).
[44] S. Wakoh, T. Fukamachi, S. Hosoya, and J. Yamashita, J. Phys. Soc. Jpn. **38**, 1601 (1975).
[45] A. H. MacDonald, W. E. Pickett, and D. D. Koelling, J. Phys. C **13**, 2675 (1980).
[46] D. G. Shankland, in *Computational Methods in Band Theory*, edited by P. Marcus, J. Janak, and A. Williams (Plenum, New York, 1971), p. 362.
[47] D. D. Koelling and J. H. Wood, J. Comput. Phys. **67**, 253 (1986).
[48] W. E. Pickett, H. Krakauer, and P. B. Allen, Phys. Rev. B **38**, 2721 (1988).
[49] R. Parker and M. Halloran, Phys. Rev. B **9**, 4130 (1974).
[50] M. R. Norman and D. D. Koelling, Phys. Rev. B **28**, 4357 (1983).
[51] S. Wakoh, J. Phys. F **7**, L15 (1977).
[52] M. van Schilfgaarde and F. Herman, Phys. Rev. Lett. **71**, 1923 (1993).
[53] J. Harris, Phys. Rev. B **31**, 1770 (1985).
[54] W. Foulkes and R. Haydock, Phys. Rev. B **39**, 12 520 (1989).
[55] M. D. Stiles, Phys. Rev. B **48**, 7238 (1993).
[56] B. Lee and Y.-C. Chang, Phys. Rev. B **52**, 3499 (1995).
[57] Z. Qui, J. Pearson, and S. Bader, J. Appl. Phys. **73**, 5765 (1993).
[58] J. C. Slater and G. F. Koster, Phys. Rev. **94**, 1498 (1954).
[59] F. Aliev *et al.*, Phys. Rev. Lett. **78**, 134 (1996).
[60] E. W. Fenton, Solid State Commun. **32**, 195 (1979).
[61] E. W. Fenton and C. R. Leavens, J. Phys. F **10**, 1853 (1980).
[62] R. S. Fishman and S. H. Liu, Phys. Rev. B **48**, 3820 (1993).
[63] J. Mathon, M. Villeret, D. Edwards, and R. Muniz, J. Magn. Magn. Mater. **121**, 242 (1993).
[64] L. Nordström, P. Lang, R. Zeller, and P. Dederichs, Phys. Rev. B **50**, R13 058 (1994).
[65] C.-Y. You *et al.*, J. Appl. Phys. (to be published).
[66] F. Herman and R. Schrieffer, Phys. Rev. B **46**, R5806 (1992).
[67] P. Bruno and C. Chappert, Phys. Rev. Lett. **67**, 1602 (1991).
[68] P. Taylor, Phys. Rev. **131**, 1995 (1963).
[69] M. Kaganov and A. Semenenko, Sov. Phys. JETP **23**, 419 (1966).